Formation of H_3^- by radiative association of H_2 and H^- in the interstellar medium

M. Ayouz,[1] R. Lopes,[1] M. Raoult,[1] O. Dulieu,[1,*] and V. Kokoouline[1,2]

[1]*Laboratoire Aimé Cotton, CNRS, Bât 505, Université Paris 11, F-91405 Orsay Cedex, France*

[2]*Department of Physics, University of Central Florida, Orlando, Florida 32816, USA*

(Received 24 February 2011; published 27 May 2011)

We develop the theory of radiative association of an atom and a diatomic molecule within a close-coupling framework. We apply it to the formation of H_3^- after the low-energy collision (below 0.5 eV) of H_2 with H^-. Using recently obtained potential energy and permanent dipole moment surfaces of H_3^-, we calculate the lowest rovibrational levels of the H_3^- electronic ground state and the cross section for the formation of H_3^- by radiative association between H^- and ortho- and para-H_2. We discuss the possibility for the H_3^- ion to be formed and observed in the cold and dense interstellar medium in an environment with a high ionization rate. Such an observation could be a probe for the presence of H^- in the interstellar medium.

DOI: 10.1103/PhysRevA.83.052712 PACS number(s): 34.50.−s, 95.30.Ft

I. INTRODUCTION

Many chemical reactions in the interstellar medium (ISM) are powered by cosmic rays: atoms and molecules (mainly molecular hydrogen) are ionized by radiation, which provides sufficient energy to initiate a chain of chemical reactions in interstellar clouds leading to the synthesis of polyatomic molecules. About 14 positive ions have been observed and identified in the ISM, including the simplest triatomic one, H_3^+. This ion plays an important role in the chemistry and evolution of interstellar clouds [1,2], as its abundance is strongly related to the production of H_2^+ in the ISM. In contrast, the existence of stable negative ions has long been thought to be impossible due to the presence of UV radiation in the ISM. In particular, the H^- ion, which has a single bound state, has not been directly detected yet, so its presence, though probable, is still controversial [3]. Although it was proposed some time ago [4], the surprise came with the detection of negative molecular ions in dense molecular clouds or carbon star envelopes. Several carbon chain ions have been detected so far: C_6H^- [5–7], C_4H^- [8], C_8H^- [9], C_3N^- [10], C_5N^- [6,7], and CN^- [11]. All these species are closed-shell systems with a quite high electron binding energy (3.8 eV for C_6H^-) and the large permanent dipole moment of several debyes. Although it is generally accepted that in the ISM these ions are formed after radiative capture of an electron by the parent neutral molecules [12], no detailed quantum mechanical treatment has been developed yet for modeling the process.

As the negatively charged counterpart of H_3^+, the H_3^- ion is predicted to be stable by about 0.013 eV [13,14]. It has never been detected so far in the cold regions of the ISM, while Wang *et al.* [15] observed it by mass spectrometry of laboratory plasmas. The H_3^- ion cannot be formed by radiative attachment from the unstable H_3 molecule, so one must consider alternative paths: three-body recombination (TBR), $H_2 + H^- + X \rightarrow H_3^- + X$, or radiative association (RA), $H_2 + H^- \rightarrow H_3^- + \hbar\omega$. The TBR mechanism must be the dominant process of H_3^- formation in laboratory plasma, but it is probably inefficient in the ISM because of low H_2 densities. The goal of this study is to investigate the possibility of forming H_3^- by RA of H_2 and H^- in low-temperature (<150 K) environments. Note that RA between H_2 and He^+ was investigated recently in a similar energy range [16].

Collisions between H^- and H_2 have been studied both theoretically [13,17] and experimentally [18,19], only for collision energies higher than 0.5 eV. In contrast, the structure of the H_3^- ion has rarely been explored in the past [13]. Recently, we calculated (see Ref. [14], hereafter referred to as paper I) a new accurate potential energy surface for the H_3^- electronic ground state, whose accuracy was improved compared to that of the previous *ab initio* calculations [13,17]. In addition, we have determined for the first time the H_3^- permanent dipole moment surface, which is needed for the RA calculations. The H_3^- ion is well represented as a loosely bound $H_2 \cdots H^-$ complex with several rovibrational states, bound by, at most, about 70 cm^{-1}. We have also found that there are a number of predissociation resonances, which can be described as excited rovibrational states (j,v) of H_2 perturbed by H^- coupled to the dissociation continuum $H_2(j',v') + H^-$ with an energy of the dimer state $E(j',v')$ lower than $E(j,v)$.

The paper is organized as follows. In the next section we discuss the geometry of the H_3^- molecule. In Sec. III we introduce the rovibrational wave functions of the molecule for bound and continuum states. The theory of RA of a dimer and an atom is developed in Sec. IV. Finally, in Sec. V we present results of numerical calculations of the RA cross section and of the rate coefficient for H_3^- formation, and we discuss the possibility of observing the H_3^- ion in the ISM.

II. REPRESENTATION OF THE $H_2 \cdots H^-$ COMPLEX AT LOW ENERGIES

The H_3^- molecule is composed of three identical nuclei, described in principle within the CNPI (complete nuclear permutation inversion) group D_{3h} [20]. However, due to the loosely bound nature of the H_3^- ion in its electronic ground state [13,14], the probability of exchange of the H^- proton with the dimer protons is negligible. Moreover, the component of the permanent dipole moment of H_3^- along the axis separating H_2 and H^- is 2 orders of magnitude

*olivier.dulieu@lac.u-psud.fr

larger than its transverse components (paper I). Therefore, low-energy collision between H_2 and H^- can be studied as an inelastic collision of two structured particles. We first define two coordinate systems: The space-fixed (SF) frame, with axes (x,y,z), and the body-fixed (BF) frame, with axes (X,Y,Z), whose orientation in the SF frame is given by the Euler angles α_e, β_e, and γ_e. The Z axis connects the center of the H_2 molecular axis with the nucleus of H^-, and its X axis is in the plane of the three nuclei. The orientation of the dimer with respect to Z is given by the azimuthal angle θ. The natural coordinate system associated with the BF frame is the Jacobi coordinate system (R,r,θ), where R is the distance between H_2 and H^- along the Z axis, and r the internuclear distance of H_2.

The quantum numbers resulting from the symmetry operations of the $C_{\infty v}$ group are well adapted to this "superdimer" approximation. The quantum numbers of the H_2 dimer are treated as good quantum numbers. The quantum states of the $H_2\cdots H^-$ complex at low energies are characterized by the quantum numbers $(J,M,j,v,\Omega^{\pm})$: J and j, associated with the total angular momentum $\widehat{\mathbf{J}}$ of the complex and with the angular momentum $\widehat{\mathbf{j}}$ of the dimer, the vibrational state v of H_2, the absolute values M and Ω of the projection of $\widehat{\mathbf{J}}$ on the SF z axis, and of $\widehat{\mathbf{j}}$ on the BF Z axis, and the intrinsic parity $\pm$ of the wave function with respect to the reflection σ_v through the plane containing the Z axis. For $\Omega \neq 0$ the Ω^+ and Ω^- states are degenerate in this approximation. If the $H_2\cdots H^-$ complex is bound, an additional quantum number v_t characterizes the vibration along the Z axis. One defines the basis set $|J,v,j,\Omega\rangle$

$$|J,v,j,\Omega\rangle = \sqrt{\frac{2J+1}{8\pi^2}}\left[D^J_{M\Omega}(\alpha_e,\beta_e,\gamma_e)\right]^* \Theta^{\Omega}_j(\cos\theta)\chi_{vj}(r), \tag{1}$$

where the normalized function $\Theta^{\Omega}_j(\cos\theta) = P^{\Omega}_j(\cos\theta)/\sqrt{4\pi}$ [21] is proportional to the associated Legendre polynomial and describes the rotational state of the dimer, and $\chi_{vj}(r)$ is the vibrational wave function of H_2. The Wigner function $D^J_{M\Omega}(\alpha_e,\beta_e,\gamma_e)$ is associated with the rotation of the complex in the SF frame. The function above is not yet symmetrized with respect to σ_v, and correspondingly, Ω can be positive or negative. Assuming that the potential energy surface $V(R,r,\theta)$ is known (see paper I), one derives the interaction matrix $\mathbf{V}$ (diagonal with respect to Ω) written in the above basis (after integration over r and θ, denoted by the subscripts to the angle braces):

$$V^J_{vj\Omega,v'j'\Omega'}(R) = \langle Jvj\Omega|V(R,r,\theta)|Jv'j'\Omega\rangle_{r,\theta}\delta_{\Omega\Omega'}. \tag{2}$$

As $R \to \infty$, the diagonal (in v and j) elements of this matrix become equal to the energies ϵ_{vj} of the rovibrational quantum states $|vj\rangle$ of H_2. The diagonalization of the $\mathbf{V}$ matrix at every R value yields a set of adiabatic potential energy curves, correlated, at large R, with the sum of ϵ_{vj} and of the H^- ground state (Fig. 1). These curves can accommodate bound levels corresponding to the quantization of the vibrational motion along the R coordinate. The H_2 nuclear spin $i_d = 0$ (para-H_2) or $i_d = 1$ (ortho-H_2) determines the possible values of j, namely, even in the former case, and odd in the latter

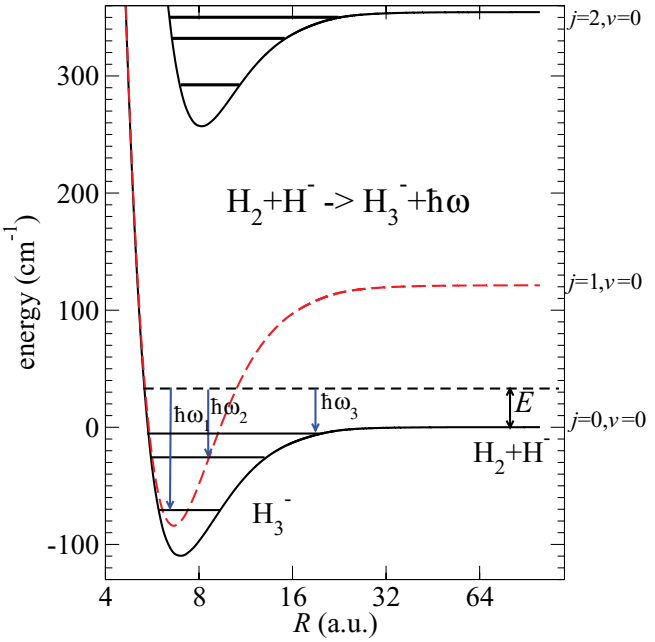

FIG. 1. (Color online) Adiabatic curves of H_3^- as functions of the Jacobi coordinate R (on a logarithmic scale), and the scheme for radiative association at a low collisional energy E. Horizontal lines indicate positions of several bound states (reported in Table I) and resonances.

case. The energy of the state does not depend on the quantum number M, which is omitted in the following.

The wave functions of Eq. (1) must be properly symmetrized with respect to σ_v and total inversion E^*, corresponding to the symmetry operators of the $C_{\infty v}$ group relevant to the present approximation. The $|J,v,j,\Omega\rangle$ functions obey the transformations

$$\begin{aligned}\sigma_v|J,v,j,\Omega\rangle &= |J,v,j,-\Omega\rangle\\ E^*|J,v,j,\Omega\rangle &= (-1)^J|J,v,j,-\Omega\rangle\end{aligned} \tag{3}$$

so we define the appropriate symmetrized combinations for $\Omega > 0$:

$$|J,v,j,\Omega^{\pm}\rangle = \left(|J,v,j,\Omega\rangle \pm |J,v,j,-\Omega\rangle\right)/\sqrt{2}\,. \tag{4}$$

From these equations, the total parity of the Ω^+ and Ω^- states is given by the value of $(-1)^J$ and $(-1)^{J+1}$, respectively. Permutation (12) of the the two nuclei of H_2 requires another symmetrization of the dimer wave functions,

$$(12) \quad |J,v,j,\Omega\rangle = (-1)^j|J,v,j,\Omega\rangle\,, \tag{5}$$

so that we can write the following four wave functions labeled by the irreducible representations (irreps) of the C_{2v} group $\Gamma = A_1,A_2,B_1,B_2$ (see Eq. (94.18) of [21]) (with $\Omega \geqslant 0$):

$$\begin{aligned}|A_1,J,v,j,\Omega\rangle = \mathcal{N}(&|J,v,j,\Omega\rangle + (-1)^j|J,v,j,\Omega\rangle\\ &+ (-1)^J|J,v,j,-\Omega\rangle\\ &+(-1)^{J+j}|J,v,j,-\Omega\rangle),\end{aligned} \tag{6}$$

$$\begin{aligned}|A_2,J,v,j,\Omega\rangle = \mathcal{N}(&|J,v,j,\Omega\rangle + (-1)^j|J,v,j,\Omega\rangle\\ &- (-1)^J|J,v,j,-\Omega\rangle\\ &-(-1)^{J+j}|J,v,j,-\Omega\rangle),\end{aligned} \tag{7}$$

$$|B_1,J,v,j,\Omega\rangle = \mathcal{N}(|J,v,j,\Omega\rangle - (-1)^j|J,v,j,\Omega\rangle - (-1)^J|J,v,j,-\Omega\rangle + (-1)^{J+j}|J,v,j,-\Omega\rangle), \quad (8)$$

$$|B_2,J,v,j,\Omega\rangle = \mathcal{N}(|J,v,j,\Omega\rangle - (-1)^j|J,v,j,\Omega\rangle + (-1)^J|J,v,j,-\Omega\rangle - (-1)^{J+j}|J,v,j,-\Omega\rangle), \quad (9)$$

where the factor $\mathcal{N}$ ensures normalization to unity. Some functions above are identically equal to 0 for certain combinations of J, j, and Ω, which means that the corresponding irreps are not allowed with these combinations.

III. BOUND AND CONTINUUM WAVE FUNCTIONS OF THE $H_2\cdots H^-$ COMPLEX AT LOW ENERGIES

The superdimer approximation above is useful for defining basis functions with the appropriate symmetry. However, the quantum numbers of the H_2 internal state can be used at large separation, but not when H_2 approaches H^-. An accurate description of the wave functions $|\Gamma,J,E\rangle$ of the $H_2\cdots H^-$ complex with energy E (E being either the collision energy or the bound-state energy of the complex) is obtained within the close-coupling framework, for which we recall below the main steps. The close-coupled expansion on $N_{\rm tot}$ symmetrized channel functions $|\Gamma,J,a\rangle$ is written as

$$|\Gamma,J;E\rangle = \sum_{a=1}^{N_{\rm tot}} C_a(E)|\Gamma,J,a;E\rangle, \quad (10)$$

where a is the channel index. The channel functions $|\Gamma,J,a;E\rangle$ are the independent solutions of the Schrödinger equation with appropriate boundary conditions. They are written as a linear combination of $N_{\rm tot}$ basis functions $|\Gamma,J,v,j,\Omega^{\pm}\rangle$

$$|\Gamma,J,a;E\rangle = \sum_{k=1}^{N_{\rm tot}} F_{k,a}(R;E)|\Gamma,J,v_k,j_k,\Omega_k\rangle. \quad (11)$$

In these expressions, the index a can be assigned to the asymptotic limit of the channel wave function in the BF frame at large distances, that is, $(a \equiv v_a,j_a,\Omega_a)$. The number of channels $N_{\rm tot}$ is determined by convergence check on the calculated physical property, namely, the binding energies or the RA cross sections.

The $F_{k,a}$ expansion coefficients are solutions of the set of coupled differential equations written (in a matrix form) in the BF frame as

$$\left[-\frac{\hbar^2}{2m}\frac{\partial^2}{\partial R^2}\mathbf{I} + (\boldsymbol{\epsilon} - E\mathbf{I}) + \mathbf{W}(R)\right]\mathbf{F}(R) = \mathbf{0}, \quad (12)$$

where m is the reduced mass of the complex, and $\boldsymbol{\epsilon}$ the diagonal matrix of the H_2 energies ϵ_{vj}. The interaction matrix $\mathbf{W}$ is the sum of the interaction potential matrix $\mathbf{V}$ [Eq. (2)] and of matrix $\mathbf{R}$ (diagonal in v and j) describing the atom-diatom relative rotation with the orbital angular momentum operator $\widehat{\boldsymbol{l}} = \widehat{\mathbf{J}} - \widehat{\mathbf{j}}$:

$$R^{\Gamma J}_{vj\Omega,v'j'\Omega'} = \langle\Gamma,J,v,j,\Omega|\widehat{\boldsymbol{l}}^2|\Gamma,J,v',j',\Omega'\rangle\frac{\delta_{vj,v'j'}}{2mR^2}. \quad (13)$$

A detailed expression of these matrix elements in the BF frame is given in Ref. [22]. The operator $\hat{\boldsymbol{l}}^2$ couples channels with different values of Ω, through long-range terms that dominate the potential energy terms due to their R^{-2} character. Therefore to treat a scattering process conveniently, it is usual to choose the representation in the SF frame where the scattering channels are fully decoupled, and where the $\hat{\boldsymbol{l}}^2$ operator is diagonal [with eigenvalues $\ell(\ell+1)$]:

$$R^{\Gamma J}_{vj\ell,v'j'\ell'} = \frac{\ell(\ell+1)}{2mR^2}\delta_{vj\ell,v'j'\ell'}. \quad (14)$$

Similarly to Eq. (10), the total wave function $|\Gamma,J;E\rangle$ in the SF frame is expressed as

$$|\Gamma,J;E\rangle = \sum_{\alpha=1}^{N_{\rm tot}} C_\alpha(E)|\Gamma,J,\alpha;E\rangle, \quad (15)$$

where the channel wave functions $|\Gamma,J,\alpha;E\rangle$ are expanded on the basis set $|\Gamma,J,v,j,\ell\rangle$

$$|\Gamma,J,\alpha;E\rangle = \sum_{\kappa=1}^{N_{\rm tot}} F_{\kappa,\alpha}(R;E)|\Gamma,J,v_\kappa,j_\kappa,\ell_\kappa\rangle. \quad (16)$$

Like the channel index a in the BF frame, the index α can be assigned at large distances to the asymptotic channel, that is, $(\alpha \equiv v_\alpha,j_\alpha,\ell_\alpha)$. The $F_{\kappa,\alpha}$ coefficients are solutions of Eq. (12) where the matrices are expressed in the SF basis set. The matrix elements of $\mathbf{V}$ in the SF frame are related to those in the BF frame according to

$$V^{\Gamma J}_{vj\ell,v'j'\ell'}(R) = \sum_{\Omega=0}^{J}\langle\ell|\Omega\rangle^{\Gamma J}V^{\Gamma J}_{vj\Omega,v'j'\Omega}(R)\langle\Omega|\ell'\rangle^{\Gamma J}, \quad (17)$$

where $\langle\ell|\Omega\rangle^{\Gamma J}$ is a matrix element of the transformation between BF and SF angular basis sets:

$$\langle\ell|\Omega\rangle^{\Gamma J} = (-1)^{J+\Omega}\sqrt{2\ell+1}\sqrt{2-\delta_{\Omega,0}}\begin{pmatrix} j & J & \ell \\ \Omega & -\Omega & 0\end{pmatrix}. \quad (18)$$

The total parity $(-1)^J$ and $(-1)^{J+1}$ for the Ω^+ and Ω^- states imposes that the sum in Eq. (16) is restricted to j and ℓ values satisfying $(-1)^J = (-1)^{j+\ell}$ and $(-1)^{J+1} = (-1)^{j+\ell}$, respectively.

At this stage, the coefficients of channel superposition in Eq. (10) are still unspecified. They are determined by applying appropriate boundary conditions when the set of differential equations of Eq. (12) is solved. Bound states are characterized by imposing the standard boundary conditions for each channel α:

$$\begin{aligned} F_{\kappa,\alpha}(0;E_t) &= 0 \quad \forall \quad \kappa \in [1,N_{\rm tot}], \\ F_{\kappa,\alpha}(R;E_t) &\overset{R\to\infty}{\longrightarrow} 0 \quad \forall \quad \kappa \in [1,N_{\rm tot}]. \end{aligned} \quad (19)$$

These quantization conditions are fulfilled only for discrete energies E_t, corresponding to a discrete vibrational level v_t of H_3^- characterizing the number of nodes (in the R coordinate) of the radial wave function in the dominant channel α_0' for given Γ and J. We used the renormalized Numerov method [23] to solve the coupled Eq. (12) written in the SF frame, so the resulting superposition coefficients $C_\alpha^{v_t}$ ensure that outward-propagated and inward-propagated wave functions are equal with identical derivatives at a well-chosen matching distance

TABLE I. Computed binding energies (in cm^{-1}) of the vibrational levels v_t ordered as rotational progressions in J, of the para-H_2–H^- complex with respect to the lowest dissociation limit H_2 ($v = 0,\ j = 0$) + H^-. Levels are labeled with the approximate quantum numbers $v = 0,\ j = 0$, and $\ell \equiv J$. Their total parity is given by $(-1)^J$.

Γ,J,v,j,ℓ,v_t	Energy	Γ,J,v,j,ℓ,v_t	Energy
A_1,0,0,0,0,0	−71.2	A_2,1,0,0,1,1	−23.8
A_2,1,0,0,1,0	−68.2	A_1,2,0,0,2,1	−20.2
A_1,2,0,0,2,0	−62.4	A_2,3,0,0,3,1	−15.0
A_2,3,0,0,3,0	−53.8	A_1,4,0,0,4,1	−8.6
A_1,4,0,0,4,0	−42.8	A_2,5,0,0,5,1	−1.7
A_2,5,0,0,5,0	−29.7	A_1,0,0,0,0,2	−5.4
A_1,6,0,0,6,0	−15.3	A_2,1,0,0,1,2	−4.5
A_1,0,0,0,0,1	−25.7	A_1,2,0,0,2,2	−2.7
		A_2,3,0,0,3,2	−0.4

[23]. Equations (15) and (16) are recast for the wave function of an H_3^- bound level $|\Gamma,J,v_t\rangle$ as

$$|\Gamma,J;\alpha_0',v_t\rangle = \sum_{\kappa'=1}^{N_{\rm tot}} \Phi_{\Gamma J\kappa'}^{\alpha_0' v_t}(R)|\Gamma,J,v_{\kappa'},j_{\kappa'},\ell_{\kappa'}\rangle, \quad (20)$$

$$\Phi_{\Gamma J\kappa'}^{\alpha_0' v_t}(R) = \sum_{\alpha'=1}^{N_{\rm tot}} C_{\alpha'}^{\alpha_0' v_t} F_{\kappa',\alpha'}(R;E_t). \quad (21)$$

As an illustration, the calculated energies of lowest H_3^- bound levels for $J = 0$ to 6 corresponding to the binding of para-$H_2(v = 0, j = 0)$ with H^- are reported in Table I, labeled with v_t and with the approximate quantum numbers v, j, ℓ of the corresponding dissociation threshold. This is justified by the weak interaction of the lowest channel ($v = 0,\ \ j = 0,\ \ell$) with the others, as already noted in paper I. There is a single dominant component in the expansion of Eq. (20). The present energies for $J = 0$ are found to be in agreement within 0.5 cm^{-1} with those obtained in paper I using a different integration method. Beyond $J = 6$ no bound level can exist below the dissociation threshold. Bound levels with energies below the ortho-H_2 ($v = 0,\ j = 1$) + H^- threshold are reported in Table II. All other bound levels, which are found at energies below thresholds with nonzero even(odd) values of j, correspond to predissociation resonances, which will decay into the continua of the H_2 ($v = 0, j'$) + H^- thresholds with j' even(odd) and $0(1) \leqslant j' < j$. All these levels are included in the RA cross-section calculations below.

Note that these results, in addition to transition dipole moments obtained from the permanent dipole moment surface, could be used to model an absorption spectrum that could guide the search for H_3^- rotational transition lines in the ISM absorption spectra in the millimeter-wavelength range. Only P and R lines ($\Delta J = \pm 1$) will be observed between levels within levels in the same part in Tables I (A_1-A_2 transitions) and II (B_1-B_2 transitions). Q transitions ($\Delta J = 0$) will connect only levels from the upper part in Table II with levels from the lower part in this table (B_1-B_2 transitions).

In a scattering process with energy E, the number of energetically open channels N_o gives the number of physical solutions of Eq. (12). The remaining $N_c = N_{\rm tot} - N_o$ closed

TABLE II. Computed binding energies (in cm^{-1}) of the vibrational levels v_t of the ortho-H_2–H^- complex ordered as rotational progressions in J, with respect to the lowest dissociation limit H_2 ($v = 0,\ j = 1$) + H^-. Levels are labeled with the approximate quantum numbers $v = 0,\ j = 1$, and ℓ. The total parity is $(-1)^J$ for the levels in the upper part and $(-1)^{J+1}$ for the levels in the lower part.

Γ,J,v,j,ℓ,v_t	Energy	Γ,J,v,j,ℓ,v_t	Energy
B_2,0,0,1,1,0	−152.7	B_2,0,0,1,1,2	−33.2
B_1,1,0,1,0,0	−149.3	B_1,1,0,1,0,2	−31.6
B_2,2,0,1,1,0	−142.6	B_2,2,0,1,1,2	−28.4
B_1,3,0,1,2,0	−132.6	B_1,3,0,1,2,2	−23.9
B_2,4,0,1,3,0	−119.7	B_2,4,0,1,3,2	−18.2
B_1,5,0,1,4,0	−104.0	B_1,5,0,1,4,2	−11.8
B_2,6,0,1,5,0	−85.8	B_2,6,0,1,5,2	−5.0
B_1,7,0,1,6,0	−65.6	B_1,1,0,1,2,0	−13.3
B_2,8,0,1,7,0	−44.0	B_2,2,0,1,3,0	−10.0
B_1,9,0,1,8,0	−21.7	B_1,3,0,1,4,0	−5.3
B_2,0,0,1,1,1	−77.8	B_2,0,0,1,1,3	−10.7
B_1,1,0,1,0,1	−75.3	B_1,1,0,1,0,3	−9.8
B_2,2,0,1,1,1	−70.5	B_2,2,0,1,1,3	−8.1
B_1,3,0,1,2,1	−63.3	B_1,3,0,1,2,3	−5.6
B_2,4,0,1,3,1	−54.2	B_2,4,0,1,3,3	−2.7
B_1,5,0,1,4,1	−43.2	B_2,0,0,1,1,4	−1.7
B_2,6,0,1,5,1	−31.0	B_1,1,0,1,0,4	−1.3
B_1,7,0,1,6,1	−17.9	B_2,2,0,1,1,4	−0.7
B_2,8,0,1,7,1	−4.9	B_1,1,0,1,0,5	−0.07
B_2,1,0,1,1,0	−13.4	B_1,4,0,1,4,0	−0.5
B_1,2,0,1,2,0	−10.2	B_2,1,0,1,1,1	−0.1
B_2,3,0,1,3,0	−5.8		

channels should lead to nonphysical long-range behavior since the related wave functions diverge asymptotically. Accordingly, the sum in Eq. (15) is restricted to the N_o open channels

$$|\Gamma,J,\alpha;E\rangle = \sum_{\alpha=1}^{N_o} C_\alpha(E) \sum_{\kappa=1}^{N_{\rm tot}} F_{\kappa,\alpha}(R;E)|\Gamma,J,v_\kappa,j_\kappa,\ell_\kappa\rangle, \quad (22)$$

and the usual boundary conditions are applied for each α to the set of coupled equations

$$\begin{gathered} F_{\kappa,\alpha}(0;E) = 0\ \forall\ \ \alpha \in [1,N_{\rm tot}], \\ F_{\kappa,\alpha}(R;E) \overset{R\to\infty}{\longrightarrow} 0\ \forall\ \alpha \in [N_o+1,N_{\rm tot}], \\ F_{\kappa,\alpha}(R;E) \overset{R\to\infty}{\longrightarrow} j(R,k_\kappa)\delta_{\kappa,\alpha} - n(R,k_\kappa)K_{\kappa,\alpha}(E) \\ \forall\ \alpha \in [1,N_o]. \end{gathered} \quad (23)$$

The standard collision matrix $\mathbf{K}(E)$ summarizes the channel interactions. The functions $j(R,k_\kappa)$ and $n(R,k_\kappa)$ are the regular and irregular spherical Bessel functions with momentum k_κ with respect to the $H_2(v_\kappa,j_\kappa,\ell_\kappa)$ + H^- limit. To be fully determined, the total wave function $|\Gamma,J,E\rangle$ must also specify the initial state of the scattering process, that is, the entrance channel α_0, through standard outgoing wave normalization:

$$C_\alpha^{\alpha_0}(E) = [\mathbf{I} - \imath\mathbf{K}(E)]^{-1}_{\alpha,\alpha_0}. \quad (24)$$

IV. CROSS SECTION FOR DIMER-ATOM RADIATIVE ASSOCIATION

RA of H^- with H_2 in an initial rovibrational level (v,j), creating H_3^- in a vibrational level v_t, with respect to a dissociation limit $H^- + H_2(v',j')$,

$$H_2(v,j) + H^- \rightarrow H_3^-(\Gamma',J',v_t(v',j')) + \hbar\omega_t, \qquad (25)$$

is shown schematically in Fig. 1 for $v=0$, $j=0$. A similar picture holds for H^- and ortho-$H_2(v=0,j=1)$ association. We limit our study to these two states, which are the only ones populated in cold and dense molecular ISM (see, e.g., Ref. [24]). The two partners approach each other with a collision energy E above the threshold. A photon with energy $\hbar\omega_t = E + E_{v_t}$ is emitted to stabilize H_3^- in the vibrational level v_t with binding energy E_t, with respect to the $H_2(v=0,j=0) + H^-$ or the $H_2(v=0,j=1) + H^-$ limits.

To obtain the RA cross section and rate coefficient, we modify the theoretical approach developed by Herzberg [25], which was later used by several authors [26–28] for RA in diatomic molecules and for photoassociation of cold atoms [29,30]. This formalism is somewhat similar to the treatment one of us used previously for the photodissociation of van der Waals systems, which can be considered as the inverse process [31]. The initial and final states are specified in the SF frame by $|\Gamma,J,E,\alpha_0\rangle$ and $|\Gamma,J,v_t,\alpha_0'\rangle$. The entrance channel index α_0 is correlated with the asymptotic quantum numbers v_0,j_0 of the initial H_2 level, and ℓ_0 specifying the initial collisional state. The final state of the created bound H_3^- molecule has a multichannel nature, but it is labeled, for convenience, with the vibrational index v_t, and the index α_0' of the dominant channel in its expansion [Eq. (20)], also related to the asymptotic quantum numbers $\alpha_0' \equiv v_0',j_0',\ell_0'$ (as in Tables I and II).

The Einstein coefficient $A^{\Gamma'J',\Gamma J}_{\alpha_0';\alpha_0}(E,v_t)$ for the process of Eq. (25) is written (in atomic units) [28]

$$A^{\Gamma'J';\Gamma J}_{\alpha_0';\alpha_0}(E,v_t) = \frac{4\omega_t^3}{3c^3} \sum_{\sigma=0,\pm1} |\langle \Gamma' J' v_t \alpha_0' | \mu^\sigma | \Gamma J E \alpha_0 \rangle|^2, \quad (26)$$

where $\mu^\sigma = \mu^0,\mu^{\pm1}$ are the three components of the permanent dipole moment operator $\widehat{\boldsymbol{\mu}}$ in the SF frame. The μ^σ components in the BF frame are related to those in the SF frame (determined in paper I) by the Wigner rotation functions D depending on the Euler angles α_e and β_e:

$$\mu^\sigma = \sum_{\lambda=0,\pm1} \left[D^1_{\sigma,\lambda}(\alpha_e,\beta_e,0)\right]^* \mu^\lambda. \qquad (27)$$

We obtain

$$A^{\Gamma'J',\Gamma J}_{\alpha_0';\alpha_0}(E,v_t) = \frac{4\omega_t^3}{3c^3}(2J+1)(2J'+1) \times \sum_{\sigma=0,\pm1} \begin{pmatrix} J & 1 & J' \\ M & \sigma & -M-\sigma \end{pmatrix}^2 \times \left| \sum_{\lambda=0,\pm1} \langle \Gamma',J';v_t,\alpha_0'|\mu^\lambda|\Gamma,J;E,\alpha_0\rangle \right|^2, \qquad (28)$$

which becomes, after averaging over the M values,

$$A^{\Gamma'J',\Gamma J}_{\alpha_0';\alpha_0}(E,v_t) = \frac{4\omega_t^3}{3c^3}(2J'+1) \times \left| \sum_{\lambda=0,\pm1} \langle \Gamma',J';v_t,\alpha_0'|\mu^\lambda|\Gamma,J;E,\alpha_0\rangle \right|^2. \qquad (29)$$

We now introduce the expressions for the total wave functions [Eqs. (20) and (22)]:

$$A^{\Gamma'J',\Gamma J}_{\alpha_0';\alpha_0}(E,v_t) = \frac{4\omega_t^3}{3c^3}(2J'+1) \times \left| \sum_{\lambda=0,\pm1} \sum_{\alpha=1}^{N_o} C^{\alpha_0}_\alpha(E) d^{\Gamma'J',\Gamma J}_{\lambda\alpha}(E,v_t,\alpha_0') \right|^2, \qquad (30)$$

with

$$d^{\Gamma'J',\Gamma J}_{\lambda\alpha}(E,v_t,\alpha_0') = \sum_{\kappa'=1}^{N'_{\rm tot}} \sum_{\kappa=1}^{N_{\rm tot}} \left\langle \Phi^{\alpha_0' v_t}_{\Gamma' J \kappa'}(R) \right| \times \mu^\lambda_{\kappa',\kappa}(R) |F_{\kappa,\alpha}(R;E)\rangle_R. \qquad (31)$$

The subscript R to the angle braces denotes integration over the R coordinate.[1] The matrix elements of the R-dependent transition dipole moment in the SF basis are

$$\mu^\lambda_{\kappa',\kappa}(R) = \sum_{\Omega'=0}^{J'} \sum_{\Omega=0}^{J} \langle \ell'|\Omega'\rangle^{\Gamma' J'} \mu^\lambda_{v'j'\Omega',vj\Omega}(R) \langle \Omega|\ell\rangle^{\Gamma J}, \qquad (32)$$

related to the matrix elements in the BF basis

$$\mu^\lambda_{v'j'\Omega',vj\Omega}(R) = (-1)^{\Omega'} \begin{pmatrix} J & 1 & J' \\ \Omega & \lambda & -\Omega' \end{pmatrix} \left\langle \chi_{v'j'}(r) \Theta^{\Omega'}_{j'}(\theta) \right| \times \mu^\lambda(R,r,\theta) \left| \chi_{vj}(r) \Theta^{\Omega}_{j}(\theta) \right\rangle_{r,\theta}. \qquad (33)$$

The subscripts r,θ to the angle braces denote integration over the r and θ variables. Note that the initial and final wave functions are not necessarily described by the same number of channels; that is, $N_{\rm tot}$ and $N'_{\rm tot}$ can be different because $J \neq J'$ and $\Gamma \neq \Gamma'$. We use energy normalization for the initial continuum state.

The probability $P^{\Gamma'J',\Gamma J}_{\alpha_0';\alpha_0}(E,v_t)$ of an RA event starting in the $|\Gamma,J;E,\alpha_0\rangle$ state with momentum $k=\sqrt{2mE}$ toward the final state $|\Gamma',J';v_t,\alpha_0'\rangle$ is given by the Einstein coefficient divided by the current density of incident particles, which is $1/(2\pi)$ for the energy-normalized wave function [21]. The corresponding RA cross section is then expressed as

$$\sigma^{\Gamma'J',\Gamma J}_{\alpha_0';\alpha_0}(E,v_t) = \pi P^{\Gamma'J',\Gamma J}_{\alpha_0';\alpha_0}(E,v_t)/k^2. \qquad (34)$$

In the following, the indexes α_0 and α_0' are assigned to their asymptotic labeling (v_0,j_0,ℓ_0) and (v_0',j_0',ℓ_0'). Physically, the

[1]Note that in the numerical implementation, the initial (energy-normalized) and final (unity-normalized) wave functions are not directly computed with the renormalized Numerov method; the integral is progressively built during the integration process, as explained in the Appendix in Ref. [31].

entrance channel is determined asymptotically by the initial rovibrational H_2 level (v_0', j_0'), so that a sum over ℓ_0 must be performed. Since nuclear spin is conserved during the RA process, there is no need to include the nuclear spin degeneracy factor. All possible final states should also be included for computation of the total RA cross section. For each initial J value, the contributions from each final value $J' = J, J \pm 1$ must be added together. At a given collision energy E, the summation over all possible values of J must be performed as well. Finally, we are interested in the formation of H_3^- in any of its stable bound levels v_t, so that the total cross section is obtained as follows:

$$\sigma_{v_0 j_0}(E) = \sum_{\Gamma J \ell_0, \Gamma' J' v_t' v_0' j_0' \ell_0'} \sigma^{\Gamma' J', \Gamma J}_{v_0' j_0' \ell_0', v_0 j_0 \ell_0}(E, v_t). \qquad (35)$$

As reported in paper I, the component $\mu^0(R,r,\theta)$ (along the Z axis) of the H_3^- dipole moment in Eq. (33) is larger by 2 orders of magnitude than the other two components $\mu^{\pm 1}(R,r,\theta)$. Therefore, the contribution from the transverse components is neglected. The total cross sections $\sigma_{00}(E)$ and $\sigma_{01}(E)$ for RA of H^- with para-H_2 $(v = 0,\ j = 0)$ and with ortho-H_2 $(v = 0,\ j = 1)$, respectively, are shown in Fig. 2. We have already mentioned that at low collision energies (below 400 cm^{-1}), a single component dominates the multichannel expansion of the initial and final wave functions. Therefore, the approximate selection rules $v_i \to v_f = v_i$, $j_i \to j_f = j_i$, and $J \to J' = J \pm 1$ hold for the RA process (with the appropriate selection rule for the parity). As expected from Eq. (29), the cross section for RA with ortho-H_2 is larger than the one with para-H_2, as the former species has a deeper potential well and has more bound states than the latter. The bumps near 1.5 cm^{-1} visible in both curves are due to the enhancement of the probability density at the top of the

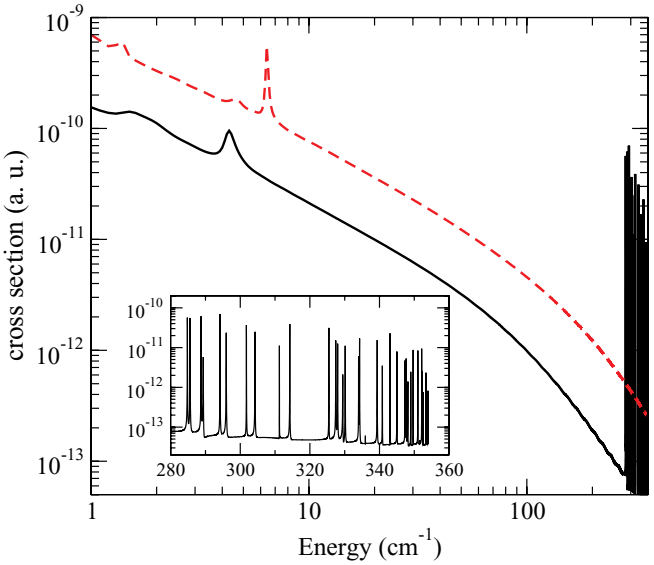

FIG. 2. (Color online) RA cross section (in atomic units) starting from para-H_2 $(v_0 = 0,\ j_0 = 0)$ (solid line) and from ortho-H_2 $(v_0 = 0,\ j_0 = 1)$ (dashed line) as a function of collision energy E above the corresponding thresholds. Inset: Enlargement of the region of Feshbach resonances induced by the bound states of the closed-channel para-H_2 $(v = 0,\ j = 2) + H^-$ (see Fig. 1).

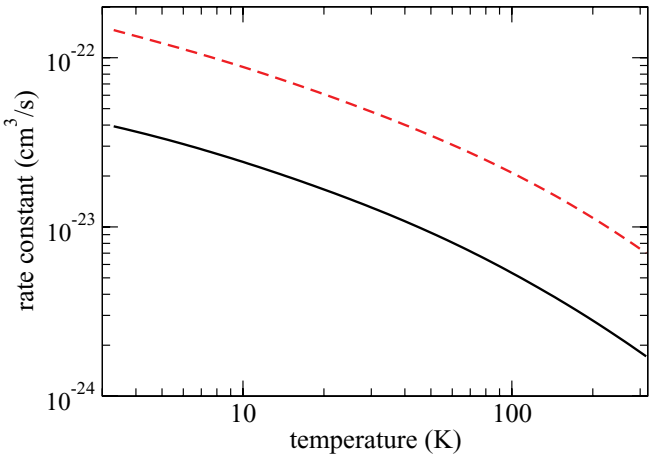

FIG. 3. (Color online) Rate coefficient k_{RA} as a function of temperature for RA of H^- with para-H_2 $(v_0 = 0,\ j_0 = 0)$ (solid line) and with ortho-H_2 $(v_0 = 0,\ j_0 = 1)$ (dashed line).

centrifugal barrier for low J. Moreover, one shape resonance is predicted near 4.3 cm^{-1} in $\sigma_{00}(E)$ and near 6.5 cm^{-1} in $\sigma_{01}(E)$ associated with nonzero J values. Once the collision energy reaches 285 cm^{-1}, at which the $j = 2$ rotational state of para-H_2 can be populated, a series of Feshbach resonances induced by the bound states of the closed-channel para-$H_2(v = 0, j = 2) + H^-$ appears in the cross section.

The RA rate coefficient $k_{RA}(T)$ is obtained by a standard integration over the Maxwell-Boltzmann collision velocity distribution. Its variation with temperature is displayed in Fig. 3 for RA of H^- with para-H_2 $(v_0 = 0,\ j_0 = 0)$ and with ortho-H_2 $(v_0 = 0,\ j_0 = 1)$. As a follow-up to Fig. 2, the rate is found to be about 4 times larger in the ortho-H_2 case than in the para-H_2 case. Note that the resonances in the latter case are too narrow to influence the rate above 200 K. The relative abundances of ortho-H_2 and para-H_2 could be out of thermal equilibrium in the interstellar clouds [24]. The obtained RA rates suggest that the ratio of ortho-H_2−H^- to para-H_2−H^- is enhanced by a factor of 4 compared to the ratio of ortho-H_2 to para-H_2.

V. DISCUSSION: IS THE FORMATION OF H_3^- IN THE ISM POSSIBLE?

The production rate of H_3^- in the ISM is directly related to the presence of H^-. Here, we propose a rough estimation of the abundance of H^- in the ISM assuming that it is formed only by dissociative attachment (DA) of an electron to H_2. Other possible mechanisms such as radiative attachment to H are neglected. The chemistry of interstellar clouds is initiated by ionization of molecular hydrogen by cosmic rays with a typical rate constant $\zeta \sim 3 \times 10^{-17}$ s^{-1} in diffuse interstellar clouds [2]. (Cloud densities are $\sim 10^2$ cm^{-3} in diffuse clouds and $\sim 10^4$ cm^{-3} in dense clouds.) The ionized molecular hydrogen H_2^+ quickly forms H_3^+ in collisions with H_2, with a rate constant $\sim 2 \times 10^{-9}$ cm^3/s [2]. The electron that escapes after ionization of H_2 has a high kinetic energy and undergoes many elastic collisions with environmental H_2 before it thermalizes. In each elastic collision with H_2, the electron loses a fraction (about $4m_e/m_{H_2}$) of its incident energy. For example, the electron should experience about

6200 elastic collisions with H_2 before its energy is decreased from 10 keV to 10 meV ($T \sim 120$ K). Possible inelastic $e^- + H_2$ collisions will lead to vibrational excitation of H_2 and to DA, $e^- + H_2 \rightarrow H + H^-$. The DA reaction is allowed for collision energies above the threshold at 3.7 eV with a cross section of about $\sigma_{DA} \sim 3 \times 10^{-21}$ cm^2 at 4 eV [32,33].

We can roughly estimate the fraction f_{DA} of escaped electrons that would form H^- rather than undergo the thermalization process. This gives us an estimate of the production rate of H^- in the ISM. The upper bound for the $e^- + H_2$ elastic cross section σ_{el} is about 1.7×10^{-15} cm^2 [34]. If we take $N_{th} = 1000$ elastic collisions corresponding to the thermalization down to the energy below which DA is impossible, we should compare σ_{el}/N_{th} with σ_{DA}. It gives approximately the value $f_{DA} = \sigma_{DA} N_{th}/\sigma_{el} \sim 0.0018$ for the fraction of escaped electrons that form H^- by DA of H_2. Therefore, the rate of H^- production (in cm^{-3}.s^{-1}) in the ISM can be estimated as $\zeta n(H_2) f_{DA} = \zeta n(H_2) \sigma_{DA} N_{th}/\sigma_{el}$. The H^- ion has only one bound electronic state and cannot be detected directly. However, if it forms a molecular ion AH^- by an association with an atom or molecule A, its presence in the ISM can be proven indirectly by rovibrational absorption spectroscopy of AH^-.

One of the motivations for this study was to investigate whether H_3^- can be formed in the ISM and be detected by photoabsorption spectroscopy. The stability of H_3^- was confirmed in this study. Therefore, H_3^- can exist in the ISM in cold clouds ($T < 100$ K). However, to be observed by far-infrared absorption spectroscopy, H_3^- should be present in the ISM in relatively large amounts. The H_3^- molecular ion and the H^- ion can be destroyed in the ISM by cosmic rays and by mutual neutralization with positive ions. These processes limit the absolute abundance of H_3^-. To determine the H_3^- abundance, one has to consider rate equations for all reactions involving formation and removal of H^- and H_3^- in the ISM. However, a rough estimation of H^- and H_3^- abundance in the ISM can be made using the available data.

First, we estimate the H^- abundance $n(H^-)$. According to our model the rate of H^- production is given by $\zeta n(H_2) f_{DA}$. The principal channel of destruction is due to the mutual neutralization with positive ions. Destruction by collisions with other negative species with higher electronic affinities is possible in principle, but their abundance is probably too low compared to those of positive ions to induce a significant loss channel. The number density n_+ of positive ions can be taken to be equal to the number density of electrons in the ISM. In diffuse clouds, the electron number density is about 0.1% of $n(H_2)$, that is, $n_+ \sim 0.01$ cm^{-3}. Therefore, the rate of removal of H^- from the ISM is $k_\pm n(H^-) n_+$ where $k_\pm$ is the rate constant for mutual neutralization. We take the value of $k_\pm \sim 10^{-7}$ cm^3/s for the $H^- + H^+ \rightarrow H + H$ reaction [35–37] at 10 meV. Therefore, we derive the equilibrium abundance of H^-: $n(H^-) = \zeta n(H_2) f_{DA}/(k_\pm n_+) \sim 5 \times 10^{-7}$ cm^{-3}. If we take the size of a cloud to be 10 pc, the resulting column density is $\sim 10^{13}$ cm^{-2}, which is a reasonable value for observation.

The estimation of H_3^- abundance $n(H_3^-)$ can be made in a similar way. The rate of H_3^- removal is determined by a similar formula: $k_\pm n(H_3^-) n_+$. The rate of H_3^- formation is $k_{RA} n(H^-) n(H_2)$. The equilibrium H_3^- abundance is then given by $n(H_3^-) = k_{RA} n(H^-) n(H_2)/(k_\pm n_+) \sim 10^{-17}$ cm^{-3}. This abundance would produce a column density that is low even for a large interstellar cloud.

If we combine the formulas for H^- and H_3^- abundances, we obtain

$$n(H_3^-) = \frac{k_{RA} \zeta f_{RA}}{(k_\pm)^2} \left(\frac{n(H_2)}{n_+} \right)^2 . \tag{36}$$

This formula suggests that the H_3^- abundance should be larger in an environment with a smaller degree of ionization (i.e., with a lower number density of positive ions). The environment should be cold enough (<100 K) for the H_3^- ion to be stable with respect to nonreactive collisions with other species (assuming, as above, that collisions with other negative species with high electronic affinities are negligible). Therefore, if H_3^- can be detected in the ISM, one has to search for it in cold, dense interstellar clouds. If H_3^- is detected, it would prove that H^- is also present in the ISM.

ACKNOWLEDGMENTS

We thank Roland Wester for motivating us to study H_3^- structure and dynamics. Stimulating discussions with Professor Jacques Robert are gratefully acknowledged. The study was supported by Triangle de la Physique as part of the project Quantum Control of Cold Molecules (Contract No. QCCM-2008-007T) and by the National Science Foundation under Grant No. PHY-0855622.

[1] T. Geballe and T. Oka, Nature **384**, 334 (1996).
[2] T. Oka, Proc. Natl. Acad. Sci. USA **103**, 12235 (2006).
[3] T. Ross, E. J. Baker, T. P. Snow, J. D. Destree, B. L. Rachford, M. M. Drosback, and A. G. Jensen, Astrophys. J. **684**, 358 (2008).
[4] E. Herbst, Nature **289**, 656 (1981).
[5] M. C. McCarthy, C. A. Gottlieb, H. Gupta, and P. Thaddeus, Astrophys. J. Lett. **652**, L141 (2006).
[6] J. Cernicharo, M. Guelin, M. Agundez, K. Kawaguchi, and P. Thaddeus, Astron. Astrophys. **61**, L37 (2007).
[7] J. Cernicharo, M. Guélin, M. Agúndez, M. C. McCarthy, and P. Thaddeus, Astrophys. J. Lett. **688**, L83 (2008).
[8] H. Gupta, S. Brünken, F. Tamassia, C. A. Gottlieb, M. C. McCarthy, and P. Thaddeus, Astrophys. J. Lett. **655**, L57 (2007).
[9] K. Kawaguchi, R. Fujimori, S. Aimi, S. Takano, E. Y. Okabayashi, H. Gupta, S. Bruenken, C. A. Gottlieb, M. C. Mccarthy, and P. Thaddeus, Publ. Astron. Soc. Japan **59**, L47 (2007).
[10] P. Thaddeus, C. A. Gottlieb, H. Gupta, S. Brunken, M. C. McCarthy, M. Agundez, M. Guelin, and J. Cernicharo, Astrophys. J. **677**, 1132 (2008).

[11] M. Agúndez *et al.*, Astron. Astrophys. **517**, L2 (2010).
[12] E. Herbst and Y. Osamura, Astrophys. J. **679**, 1670 (2008).
[13] J. Stärck and W. Meyer, Chem. Phys. **176**, 83 (1993).
[14] M. Ayouz, O. Dulieu, R. Guérout, J. Robert, and V. Kokoouline, J. Chem. Phys. **132**, 194309 (2010).
[15] W. Wang, A. Belyaev, Y. Xu, A. Zhu, C. Xiao, and X.-F. Yang, Chem. Phys. Lett. **377**, 512 (2003).
[16] F. Mrugala, W.-P. Kraemer, J. Chem. Phys. **122**, 224321 (2005).
[17] A. N. Panda and N. Sathyamurthy, J. Chem. Phys. **121**, 9343 (2004).
[18] H. Müller, Z. Zimmer, and F. Linder, J. Phys. B **29**, 4165 (1996).
[19] R. Wester, J. Phys. B **42**, 154001 (2009).
[20] P. R. Bunker and P. Jensen, *Molecular Symmetry and Spectroscopy* (NRC Research Press, Ottawa, Canada, 1998).
[21] L. Landau and E. Lifshitz, *Quantum Mechanics: Non-relativistic Theory* (Butterworth Heinemann, Burlington, MA, 2003).
[22] J. M. Launay, J. Phys. B **9**, 1823 (1976).
[23] B. R. Johnson, J. Chem. Phys. **69**, 4678 (1978).
[24] B. L. Rachford *et al.*, Astrophys. J. Suppl. Ser. **180**, 125 (2009).
[25] G. Herzberg, *Spectra of Diatomic Molecules* (Van Nostrand, New York, 1950).
[26] B. Zygelman and A. Dalgarno, Astrophys. J. **365**, 239 (1990).
[27] P. C. Stancil, J. F. Babb, and A. Dalgarno, Astrophys. J. **414**, 672 (1993).
[28] F. A. Gianturco and P. G. Giorgi, Astrophys. J. **479**, 560(1997).
[29] R. Côté, E. J. Heller, and A. Dalgarno, Phys. Rev. A **53**, 234 (1996).
[30] P. Pillet, A. Crubellier, A. Bleton, O. Dulieu, P. Nosbaum, I. Mourachko, and F. Masnou-Seeuws, J. Phys. B **30**, 2801 (1997).
[31] I. Fourré and M. Raoult, J. Chem. Phys. **101**, 8709 (1994).
[32] G. J. Schulz and R. K. Asundi, Phys. Rev. Lett. **15**, 946 (1965).
[33] J. Horácek, M. Cízek, K. Houfek, P. Kolorenc, and W. Domcke, Phys. Rev. A **70**, 052712 (2004).
[34] J. Furst, M. Mahgerefteh, and D. E. Golden, Phys. Rev. A **30**, 2256 (1984).
[35] D. R. Bates and J. T. Lewis, Proc. Phys. Soc. London Sec. A **68**, 173 (1955).
[36] B. Peart and D. A. Hayton, J. Phys. B **25**, 5109 (1992).
[37] R. K. Janev, C. L. Liu, J. G. Wang, and J. Yan, Europhys. Lett. **74**, 616 (2006).